Synthesis, Characterization and Enhanced Dielectric Constant of Polyaniline-Exfoliated Graphite Flakes Composites

Prasanna B P[a,b,*], Avadhani D N[c], Muralidhara H B[d], Revanasiddappa M[e]

[a]*C.M.R.T.U. Research Centre, R.V. College Campus, Bangalore, affiliated to Tumkur University, Tumkur 572 101, India*
[b]*Department of Physics, School of Engineering and Technology, Jain University, Bangalore 562 112, India*
[c]*Department of Physics, R.V. College of Engineering, Bangalore 560 059, India*
[d]*Centre for Emerging Technologies, Jain University, Bangalore 562 112, India*
[e]*Department of Chemistry, PESIT Bangalore South Campus, Bangalore 560 100, India*

[a,b]prasannabp2@gmail.com, [c]avadhanidn@rvce.edu.in, [d]hb.murali@gmail.com, [e]revum75@gmail.com

***Abstract*:- Polyaniline/exfoliated graphite flakes (PANI/EGF) composites have been synthesized through in situ polymerization of aniline monomer in the presence of exfoliated graphite flakes. Exfoliated graphite flakes were prepared by treating the expanded graphite with sonication in aqueous alcohol solution. The composite formation and structural changes in PANI/EGf composites were investigated by X-ray diffraction (XRD), scanning electron microscopy (SEM) and Fourier transform infrared spectroscopy (FT-IR). XRD clearly indicates the typical graphite peaks in PANI. SEM of the composites showed that EGf dispersed in the PANI matrix. The FT-IR analysis revealed there was strong interaction between PANI and EGf. Room temperature AC conductivity and dielectric response of the composites were studied in the frequency range of 100 Hz to 1 MHz. AC conductivity is independent of frequency at low frequencies and increased with increasing wt% of EGf in PANI. The dielectric constant shows unusual response with respect to frequency with very high dielectric constant of 7.92×10^6 at 1 kHz for 25 wt% of EGf in PANI, which attributes to the stronger localization of charge carriers and electrical relaxation processes. Dielectric loss in these composites depend on the content of EGf which decreases sharply with increase in wt.% of EGf in PANI.**

Keywords-Polyaniline; Exfoliated graphite, Polymerization, Dielectric loss, Composites

I. INTRODUCTION

Conducting electroactive polymers have attracted considerable attention in recent years due to a great variety of applications in many technical fields, such as electrochromism, sensors, electroluminescence, electrochemical displays, catalysis, redox capacitors, antistatic coatings and secondary batteries (1-7).

Among all conducting polymers, conducting polyaniline (PANI), as one of the heteroatomic conducting polymers, has attracted considerable attention because of its interesting electrical conductivity, novel electronic structure and mechanism of electrical conductivity as well as the possibility for application as a new electronic material. PANI exists in a number of forms which totally differ in chemical and physical properties. The most common green protonated conducting emeraldine salt has conductivity on a semiconductor level of the order of 10^0 S cm^{-1}, many orders of magnitude higher than that of traditional polymers ($<10^{-9}$ S cm^{-1}) but lower than that of metals ($>10^4$ S cm^{-1}). Also PANI is unique among conductive polymers, its electrical properties could be reversibly controlled both by charge transfer doping and by protonation (8-11). For most doped PANI, the conductivity is typically less than 10^2 S cm^{-1} and usage of PANI in electronic devices not realistic because charge carriers mobility is too low to be useful. Graphite flakes, which are naturally abundant and low cost, have been widely used as electronically conducting filler in preparing conducting polymer composites (12-14). Moreover, graphite has layered structure like that of silicates (e.g., montmorillonite and vermiculite). If PANI can be intercalated into the interlayer space of graphite, both the physiochemical properties and the electrical conductivity are expected to be improved (15, 16). Because of the small interspacing of 3.35 Å, graphite layers lack the affinity and space for hydrophilic or hydrophobic polymers. Thus it is difficult to prepare conductive polymer/graphite nanocomposites via direct intercalation. To achieve the nanoscale dispersion of graphite in a polymer matrix, a certain chemical or physical modification to the graphite is generally needed. Exfoliated graphite (property-improved graphite) consists of a large number of delaminated graphite sheets. The electrical conductivity is not obviously affected in comparison with the original graphite. Therefore monomers and polymers can be intercalated into the pores and galleries of the graphite sheets in exfoliated graphite to produce polymer/graphite conductive nanocomposites. With a similar method, polymer/graphite composites or nanocomposites with good electrical conductivity and highly thermal storage properties have been disclosed recently (17-22). The composites of PANI and graphene based materials have already been used as electrode materials in supercapacitors and counter electrode in dye-sensitized solar cells (23-25). It is envisaged that highly dispersed PANI nanoparticles covering on the graphene surface should be able to provide high conductivity as well as

good electrocatalytic activity for the use as an efficient counter electrode (23).

In the present study, conductive fillers, that is, exfoliated graphite flakes were prepared via both chemical and physical treatments of natural graphite to fabricate PANI/exfoliated graphite flakes and we present our experimental data on the evaluation of AC conductivity and dielectric properties of PANI nanocomposites containing exfoliated graphite flakes in order to suggest their applications electronic and related industries.

II. EXPERIMENTAL

a) Materials:

All the reagents used in the experiments, Aniline ($C_6H_5NH_2$), ammonium peroxydisulfate ($(NH_4)_2S_2O_8$), natural graphite, sulfuric acid (H_2SO_4), hydrochloric acid (HCl), hydrogen peroxide (H_2O_2), ethanol (C_2H_5OH) were of analytical grade and purchased from s.d. Fine Chemicals, Mumbai, India. Aniline monomer was doubly distilled before use. Deionized water was used throughout the work.

b) Preparation of Exfoliated Graphite flakes:

Exfoliated graphite flakes (EGf) were prepared as described in (13, 17). The preparation method was illustrated in Figure 1. The solution of concentrated sulfuric acid and hydrogen peroxide (1:0.08v/v) was mixed with natural graphite. The mixture was stirred at the ambient temperature for about 1 h. The as-treated graphite was carefully washed and filtered with deionized water until the pH level of the filtrate reached 6, and it was then dried at 100 °C for 24 h, the resulting graphite was subjected to a thermal shock at 1050 °C for 15 s in a muffle furnace. As prepared 1g of graphite powder was mixed and saturated with 400 ml of alcohol and distilled water with a ratio of 65:35 solution for 12 h. Then the mixture was subjected to ultrasonic irradiation with a power of 100 W for various times. After hours of sonication, graphite particles were effectively fragmented into exfoliated graphite flakes. The EGf dispersion was then filtered and dried at 80 °C to remove residue solvents. When an ultrasonic wave passes through a liquid medium, ultrasonic cavitation will take place. Ultrasonic cavitation can generate a very vigorous environment and because of the multiple effects of ultrasound, we could breakdown the expanded graphite worm and then get exfoliated graphite flakes.

c) Preparation of Polyaniline/Exfoliated graphite flakes composites:

Polyaniline/Exfoliated graphite flakes (PANI/EGf) composites were prepared by incorporating EGf into PANI matrix via in situ polymerization method (shown in Figure 1). Aniline (0.1 M) was dissolved in 30 mL of HCl (1 M) and added to 10 mL of 95% of alcohol solution. Finely ground EGf powder taken in different (5, 10, 15, 20 and 25) wt.% with respect to aniline concentration was added to the above mixture and sonicated for 1h. Then, pre-cooled solution of ammonium peroxydisulfate (0.1 M) dissolved in 40 mL of HCl (1 M) was slowly added to the above mixture under vigorous stirring over a period of 2 h. The reaction was allowed to proceed for 24 h. At the end of the reaction, PANI/EGf composite formed was collected by filtration, washed with distilled water and alcohol repeatedly until filtrate was colorless. The collected composite was dried at 80° C until constant weight was attained. Pure PANI was synthesized in the same manner in the absence of EGf.

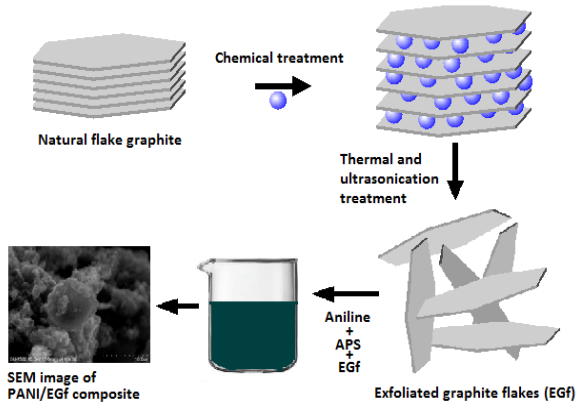

Figure 1 Schematic illustration of the synthesis of EGf and PANI/EGf composites

d) Measuring Methods:

X-ray diffraction spectra of PANI, EGf and PANI/EGf composites were recorded on a Shimidzu/7700X-ray diffractometer using Cu Kα radiation (λ = 1.5406Å) at a scanning rate of 2.0°/min using a voltage of 40 kV and a current of 30 mA. SEM images of PANI and PANI/EGf composites were recorded using the Hitachi/SU-520 scanning electron microscope. Fourier-transform infrared spectra (FTIR) of the samples were recorded on Thermo Nicolet Avatar/370 spectrometer. AC conductivity and dielectric response were measured using the samples, were prepared as 1 cm diameter pellets by pressing the powder under a hydraulic pressure of 10,000 psi and then applying conducting silver paste to form the electrodes in contact with the two circular faces. The sample was then held between two nominally spring loaded copper plates and the dielectric parameters were measured at 300K using Hioki (Japan) Model 3532-50 programmable LCR meter at the selected frequencies in the range from 100 Hz to 1 MHz

III. RESULTS AND DISCUSSIONS

a) X-ray Diffraction Studies:

Figure 2 shows the XRD of pure PANI, EGf and PANI/EGf composite. Analysis of X-ray diffraction pattern of PANI in Figure 2A shows broad peak centered at 2θ=25.6°, which suggests semi-crystalline nature of PANI (26). Figure 2B shows a typical graphite pattern and the two diffraction peaks

centered at 2θ=26.38° and 2θ=54.48°correspond to graphite's (0 0 2) and (1 1 0) planes respectively, similarly Figure 2C & 2D shows XRD of PANI/EGf-15% and PANI/EGf-20% composites respectively. The diffraction peaks of graphite located at 2θ=26.62° and 2θ=54.54° were clearly observed in the composite. Average crystalline size was calculated by using Scherrer's formula, $D=0.9\lambda/\beta\cos\theta$, where β is the line broadening at the full-width at half maximum (FWHM) of the most intense peak (0 0 2), θ is the Bragg angle and λ is the X-ray wavelength. The calculated average crystalline sizes of EGf and PANI/EGf 20wt% were found to be 22.43 and 18.53 nm, respectively. The relative intensity of graphite in the PANI/EGf composites were weakened compared with that of the graphite due to encapsulation bye PANI (29) and also it is confirmed that graphite has retained its structure even though it is dispersed in PANI during polymerization reaction.

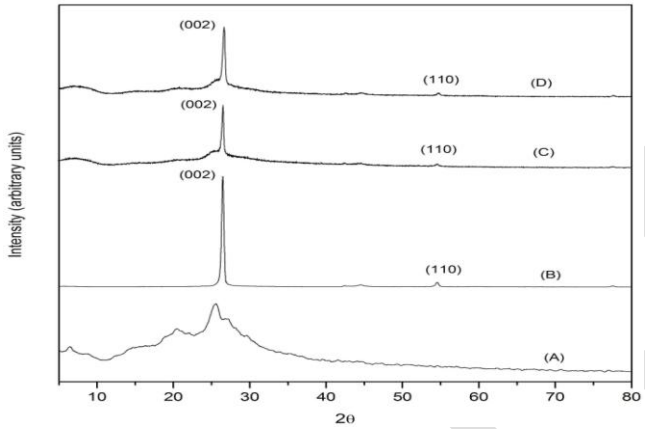

Figure 2 X-ray diffraction spectra of: (A) Pure PANI, (B) EGf, (C) PANI/EGf-15% and (D) PANI/EGf-20%.

b) Scanning Electron Microscopy

Figure 3A shows the SEM image of pure PANI with the formation of a spongy irregular agglomerated structure. Fig 3B shows the SEM image of exfoliated graphite flakes prepared using ultrasonic irradiation. Clearly, exfoliated graphite worms have been completely torn into flakes of 4–8μm in diameter. Fig 3C & 3D shows the SEM image of the EGf dispersed in PANI matrix with different wt%. Furthermore, the presence of EGf covered by polyaniline chain agglomerates and the microstructure shows the presence of modified aggregate porous regions which may facilitate good electrical conductivity and dielectric response for the composites.

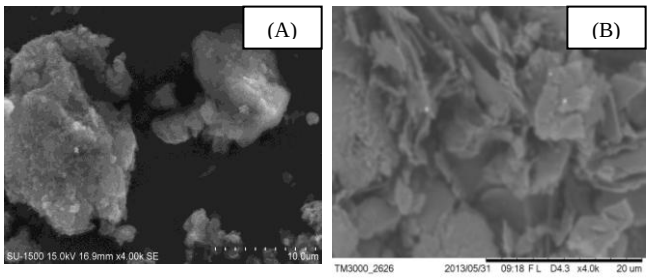

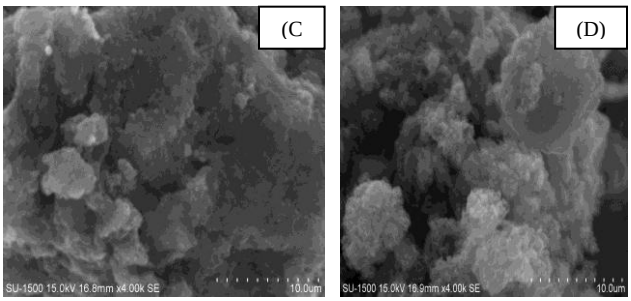

Figure 3 Scanning electron micrographs of: (A) Pure PANI, (B) EGf, (C) PANI/EGf-15% and (D) PANI/EGf-20% composites

c) FT-IR Spectroscopy:

Figure 4 shows the FT-IR spectra of pure EGf, PANI as well as PANI/EGf composite. Numerous peaks corresponding to respective functional groups are observed in the FT-IR spectra. Fig 4A represents pure EGf in absence of any organic moiety. In contrast, the spectrum corresponding to pure polyaniline (Figure 4B) shows various characteristic peaks including the peaks at 1568 and 1444 cm^{-1} representing the C-C stretching of the benzenoid and quinoid moiety (30). Peak at 3234 cm^{-1} indicates the presence of N-H stretching mode while peaks at 1296 cm^{-1} refer to C-N stretching of secondary amine (30). Figure 4C refers to PANI/EGf composite. The peak at 3455 cm^{-1} is characteristic for PANI while peaks at 1564 and 1483 cm^{-1} are attributed to benzenoid and quinoid moiety and the sharp peak at 1246 cm^{-1} represents C-N stretching vibrations. The peak intensity of PANI/EGf nanocomposite decreases with respect to PANI, indicates the interaction with EGf.

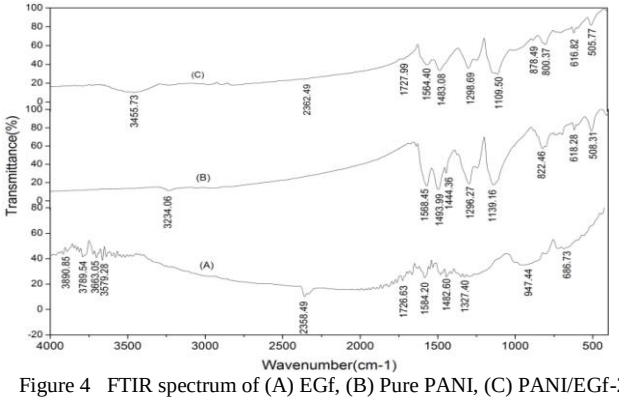

Figure 4 FTIR spectrum of (A) EGf, (B) Pure PANI, (C) PANI/EGf-20% composites.

d) AC conductivity and Dielectric properties

AC conductivity and dielectric parameters have been calculated using the values of equivalent parallel capacitance, C_p, impedance, Z and phase angle, δ, recorded by the LCR meter at a selected frequency, f, using the following equations.

$$\varepsilon' = \frac{d\,C_p}{A\varepsilon_0}$$

$$\varepsilon'' = \varepsilon' \tan\delta$$

$$or\ \tan\delta = \frac{\varepsilon'}{\varepsilon''}$$

$$\sigma'(\omega) = \omega\varepsilon_0\varepsilon''$$

$$\sigma''(\omega) = \omega\varepsilon_0\varepsilon'$$

where, C_p, the capacitance measured in pf; A and d the area and thickness of the samples, respectively; $\tan\delta$, dielectric loss with δ being phase angle. The ε' and ε'' are, respectively, the real and imaginary parts of the complex dielectric constant $\varepsilon(f) = \varepsilon'(f) - i\varepsilon''(f)$. similarly, σ' and σ'' are, respectively, the real and imaginary parts of the complex AC conductivity, $\sigma(f) = \sigma'(f) - i\sigma''(f)$.

Figure 5 shows the frequency dependent conductivity of PANI/EGf composites. At low frequency region, the composite exhibit highest electrical conductivity of 0.265 S/cm (shown in Table 1) at 25 wt% of EGf in PANI, which may be due to formation of conductive path by EGf in PANI matrix and conductivity is independent of frequency, approaching the dc conductivity at a constant value. At high frequency region the conductivity is decreases with frequency is may be depending on degree of protonation, percent crystallinity, crystalline domain size and order in crystalline and amorphous regions have relationship with the delocalization length (28). The AC response of pure PANI (inset of Figure 5) exhibits a frequency independent conductivity at low frequency region followed by a frequency dependent dispersed region obeyed the power law indicating the universal behavior of the AC conductivity in disordered media (26). The dependence of conductivity on composition is shown in Figure 6, which gives the plot of conductivity (f=10 kHz) as a function of wt% of EGf of the composite. Notice that conductivity increases with increasing wt% of EGf of the composite is could be due to conducting pillars of EGf in PANI matrix.

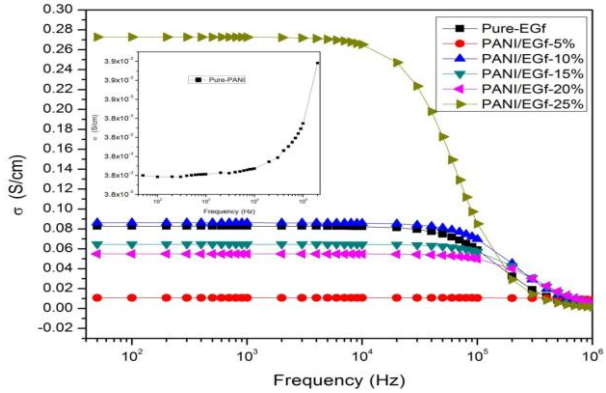

Figure 5 Frequency dependence of AC conductivity of PANI/EGf composites. *Inset*: Frequency dependence of AC conductivity of pure PANI.

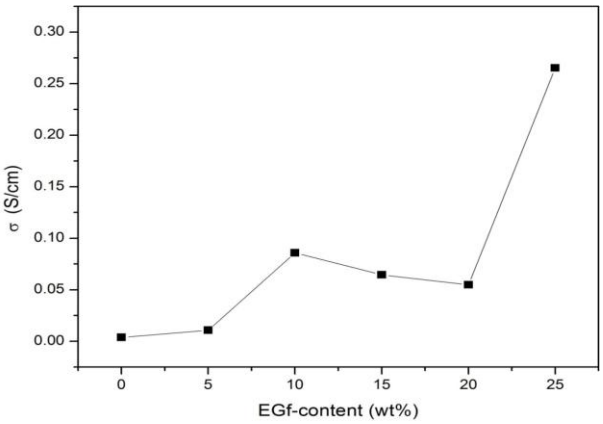

Figure 6 Variation of AC conductivity of PANI/EGf composite at 10 kHz with EGf content in the composite

Figure 7 shows the variation of real part of dielectric constant (ε') with frequency (f) for pure PANI and PANI/EGf composites. For pure PANI the real dielectric constant has a value of about 6.83×10^3 at 1 kHz, which decreases with frequency, reaching a value of 1.04×10^3 at 1 MHz. Such values of real permittivity are related to effects of electrode polarization and space charge polarization. PANI is a semiconducting system with mobile polaron/bipolaron, upon increase in the frequency of the applied field, the dipoles present in the system cannot reorient themselves quickly in response to the applied field reducing the dielectric constant (26). Dielectric constant of PANI/EGf composites are dependent on composition, protonation, temperature and delocalization length. Dependence of ε′ with frequency of the composites can be classified into three stages. In the first stage, ε′ increases with the increase of frequency within the range of 100 to 700 Hz. In the second stage, from 800 to 3 kHz, ε′ is almost constant with a value of 8.02×10^5 in PANI composites with a particle loading higher than 10 wt%. However, ε′ is significantly lower value for the pure PANI ($\sim6.83\times10^3$) and very high value (shown in Table 1) for 25 wt% EGf in PANI composite (7.92×10^6), which attributes to the stronger localization of charge carriers. In the third stage, the decrease of ε′ above 4 kHz frequency may be attributed to the electrical relaxation processes, i.e., the momentary delay in the dielectric constant of a material with respect to a change in the electric field (27-28). Dependence of ε′on composition is shown in Figure 8, which gives a plot of ε′ (f = 1, 10 and 50 kHz) as a function of wt.% of EGf in PANI. It is seen that ε′ increases with increasing concentration of EGf up to 10 wt.% and decreases for 15 and 20 wt% and again steeply increases for 25 wt.% of EGf. This is due to accumulation of charge carriers in the internal surface of PANI matrix which can be explained by Maxwell-Wagner–Sillars affects. Thus, according to the Maxwell-Wagner-Sillars model external electric field application provokes the charge carriers that can easily migrate to the grains and these grains accumulated at the grain boundaries. This process may lead to produce large polarization and high dielectric constant (29).

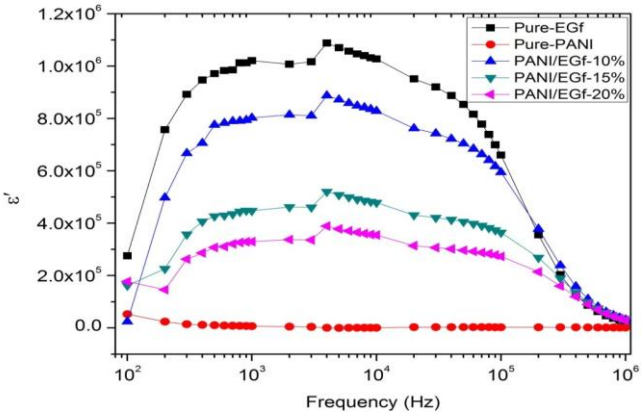

Figure 7 Frequency dependence of real dielectric constant of PANI/EGf composites.

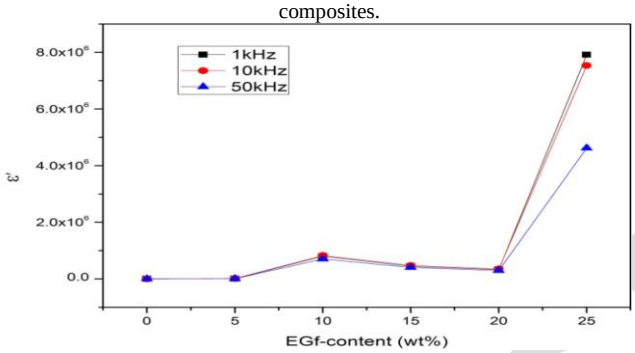

Figure 8 Variation of real dielectric constant of PANI/EGf composite at different frequencies with EGf content in the composite.

The dielectric loss, tan δ, as a function of frequency for PANI/EGf composites is shown in Figure 9 The loss tangent for pure PANI (not shown in Figure 9) has a rather high value of 542.59 at 1 kHz (shown in Table 1), which decreases with increasing frequency, reaching a value of 0.56 at 1 MHz. It is observed from the Figure 9; high dielectric loss at low frequency in all the composites may be attributed to the high resistivity caused by grain boundary (31). The loss tangent at 1 kHz and 10 kHz taken from these graphs is shown in Table 1 and is plotted as a function of composition in the inset of Figure 9. The tangent loss decreases sharply as wt.% of EGf increases in PANI and showing very much less than that of pure PANI revealed that these nanocomposites suitable for electronic applications such as fabrication of capacitors (32).

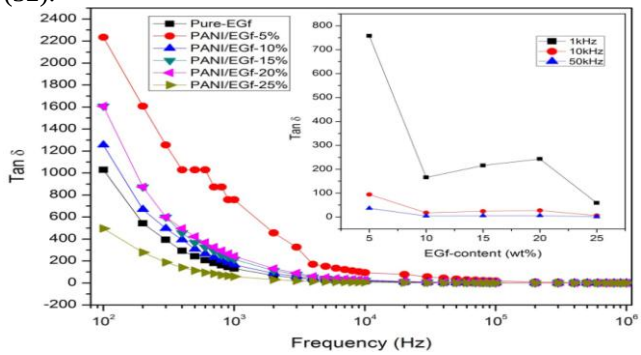

Figure 9 Frequency dependence of dielectric loss of PANI/EGf composites. *Inset*: Variation of dielectric loss of PANI/EGf composite at different frequencies with EGf content in the composite.

The complex impedance plots of pure PANI, EGf and PANI/EGf composite are shown in Figure 10 and inset of Figure 10 respectively. It is apparent that the plot of pure PANI presents a single semicircle in the low frequency region for which Debye relaxation model may be considered and the plot of EGf and PANI/EGf composite do not present semicircle, probably due to the low faradaic charge transfer resistances. EGf and PANI/EGf composite exhibits higher slope line at low-frequency, illustrating better capacitive behavior and lower diffusion resistance of ions (33).

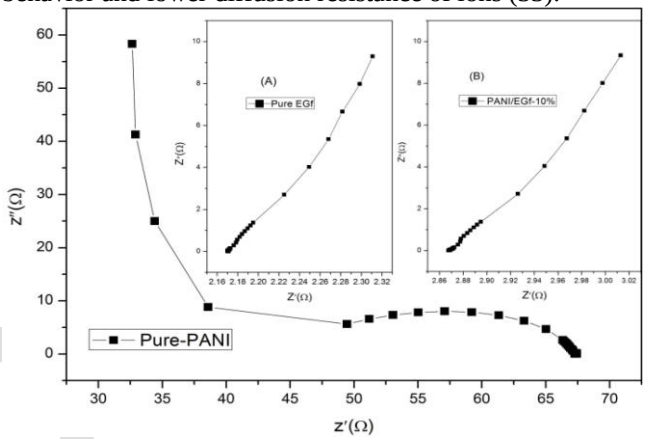

Figure 10 Complex impedance plot for pure PANI. *Inset*: (A) Impedance plot for EGf and (B) Impedance plot for PANI/EGf composite.

TABLE I - SUMMARY OF AC CONDUCTIVITY AND DIELECTRIC RESPONSE OF PANI/GNS COMPOSITES

Composition (wt.% of EGf)	Real conductivity , σ	Real dielectric constant, ε'		Dielectric loss, tan δ	
	at 10 kHz	at 1 kHz	at 10 kHz	at 1 kHz	at 10 kHz
0	0.00379	6.83×10^{3}	9.27×10^{2}	542.59	456.23
5	0.01071	9.52×10^{3}	1.88×10^{4}	757.77	94.65
10	0.08579	8.02×10^{5}	8.28×10^{5}	165.85	18.32
15	0.06449	4.48×10^{5}	4.79×10^{5}	215.79	23.82
20	0.0548	3.29×10^{5}	3.55×10^{5}	243.26	27.21
25	0.26525	7.92×10^{6}	7.54×10^{6}	58.75	6.29

IV. CONCLUSIONS

In this paper, the synthesis, composite formation and structural changes of PANI/EGf composites have been investigated. Exfoliated graphite flakes were synthesized using ultrasonic irradiation method. The PANI/EGf composites can be fabricated by in situ polymerization of aniline in the presence of EGf via ultrasonic technique. Results showed that the EGf was with diameter of 4-8μm, the dispersion of graphite flakes in the PANI matrix and clear indication of graphite peaks in PANI was evidenced by SEM and XRD examinations; there was interaction between PANI and EGf particle from FT-IR spectra analysis. AC conductivity is independent of frequency, approaching the dc conductivity at constant value and found to exhibit very high conductivity of 0.265 S/cm at 25 wt%, which could be due to conductive pillars of EGf in PANI

matrix. The composites showed some interesting dielectric response with very high dielectric constant at low frequency region and strong dependence on content of EGf in PANI matrix. It is observed that at low frequencies dielectric constant was found to increase with increasing frequency and then above 4 kHz dielectric constant is found to decrease with increase in frequency, which is the characteristic feature of disordered materials.

ACKNOWLEDGEMENTS

The authors would like to thank Department of chemistry and Department of NonoBioscience, Jain University for providing part of instrumental facility

REFERENCES

[1]. Rupali Gangopadhyay, Ankan Dutta Chowdhury, Amitabha. (2012) Functionalized polyaniline nanowires for biosensing. Sens. Actuators A :Chem. 171-172:777-785.

[2]. Jian-Gan Wang, Ying Yang, Zheng-Hong Huang, Feiyu Kang. (2012) Interfacial synthesis of mesoporous MnO_2/polyaniline hollow spheres and their application in electrochemical capacitors. J. Power Sources 204:236-243.

[3]. Liuan Gu, Jingyu Wang, Rong Qi, Xiaoyu Wang, Ping Xu, Xijiang Han. (2012) A novel incorporating style of polyaniline/TiO_2 composites as effective visible photocatalysts. J. Mol. Catal. A: Chem. 357:19-25.

[4]. H. Kebiche, D. Debarnot, A. Merzouki, F. Poncin-Epaillard, N. Haddaoui. (2012) Relationship between ammonia sensing properties of polyaniline nanostructures and their deposition and synthesis methods. Anal. Chim. Acta 737:64-71.

[5]. Khalil Arshak, Vijayalakshmi Velusamy, Olga Korostynska, Kamila Oliwa-Stasiak, Catherine Adley. (2009) Conducting polymers and their applications to biosensors: Emphasizing on foodborne pathogen detection. IEEE Sens. J. 9:1942-1951.

[6]. Meng Chen, Chunyu Du, Long Wang, Geping Yin, Pengfei Shi. (2012) Silicon/graphite/polyaniline nanocomposite with improved lithium-storage capacity and cyclability as anode materials for lithium-ion batteries. Int. J. Electrochem. Sci. 7:819-829.

[7]. Yan Li, Hongrui Peng, Guicun Li, Kezheng Chen. (2012) Synthesis and electrochemical performance of sandwich-like polyaniline/graphene composite nanosheets. Eur. Polym. J. 48:1406-1412.

[8]. K. C. Sajjan, Muhammad Faisal, Khened B. S & Syed khasim, (2013) Electrical conductivity, dielectric behavior and humidity sensing properties of polyaniline-graphite oxide composites. Int. J. Electrical and Electronics Eng.;2:67-76.

[9]. Jiahua Zhu, Minjiao Chen, HonglinQu, Xi Zhang, Huige Wei, ZhipingLuo, Henry A. Colorado, Suying Wei, Zhanhu Guo. (2012) Interfacial polymerized polyaniline/graphite oxide nanocomposites toward electrochemical energy storage. Polymer 53:5953-5964.

[10]. Xinming Wu, Shuhua Qi, GuochengDuan, (2011) Preparation and characterization of electromagnetic polyaniline/nickel plating graphite nanosheets composites through ultrasonic irradiation. Synth. Met. 161:2215-2219.

[11]. Yongqing Yang, Shuhua Qi, Yunchuan Qin, Xinxin Zhang. (2012) Synthesis and characterization of silver-coated graphite nanosheets with pyrrole via in situ polymerization. J. Appl. Polym. Sci. 125:E388-E397.

[12]. X. Wu, S. Qi, J. He, G. Duan. (2010) High conductivity and low percolation threshold in polyaniline/graphite nanosheets composites. J. Mater. Sci. 45:483-489.

[13]. Guohua Chen, WenguiWeng, Dajun Wu, Cuiling Wu, Jinrong Lu, Pingping Wang, Xiangfeng Chen. (2004) Preparation and characterization of graphite nanosheets from ultrasonic powdering technique. Carbon 42:753-759.

[14]. Weifu Sun, Guohua Chen and Lilong Zheng. (2008) Electroless deposition of silver particles on graphite nanosheets. Scripta Mater. 59:1031-1034.

[15]. Guilei Sun, Xiaojie Li, YandongQu, Xiaohong Wang, Honghao Yan, Yueju Zhang. (2008) Preparation and characterization of graphite nanosheets from detonation technique. Mater. Lett. 62:703-706.

[16]. Xinming Wu, Shuhua Qi, Jie He, Bo Chen, Guochen Duan. (2009) Synthesis of high conductivity polyaniline/Ag/graphite nanosheet composites via ultrasonic technique. J. Polym. Res. 17:751-757.

[17]. X. S. Du, M. Xiao, Y. Z. Meng. (2004) Synthesis and characterization of polyaniline/graphite conducting nanocomposites. J. Polym. Sci., Part B: Polym. Phys. 42:1972-1978.

[18]. C. Basavaraja, Won Jung Kim, P. X. Thinh, Do Sung Huh. (2012) Charge transport properties of polyaniline-gold/graphite oxide composite films. Bull. Korean Chem. Soc. 33:449-453.

[19]. Qi Li, Guo-Zhen Zeng, Wei-Feng Zhao, Guo-Hua Chen. (2010) Preparation and characterization of nickel-coated graphite nanosheets. Synth. Met. 160:200-202.

[20]. Guohua Chen, Dajun Wu, Wengui Weng, Cuiling Wu. (2003) Exfoliation of graphite flake and its nanocomposites. Carbon 41:619-621.

[21]. Shawn Bourdo, Zhongrui Li, Alexandru S. Biris, Fumiya Watanabe, Tito Viswanathan, Ioana Pavel. (2008) Structural, electricaland thermal behavior of graphite-polyaniline composites with increased crystallinity. Adv. Funct. Mater. 18:432-440.

[22]. Wenge Zheng, Shing-Chung Wong. (2003) Electrical conductivity and dielectric properties of PMMA/expanded graphite composites. Compos. Sci. Technol. 63:225-235.

[23]. Kai Zhang, Li Li Zhang, X. S. Zhao, Jishan Wu. (2010) Graphene/Polyaniline nanofiber composites as supercapacitor electrodes. Chem. Mater. 22:1392-1401.

[24]. Guiqiang Wang, Wei Xing, Shuping Zhuo. (2012) The production of polyaniline/graphene hybrids for use as a counter electrode in dye-sensitized solar cells. Electrochim. Acta 66:151-157.

[25]. Pingping Yu, Yingzhi Li, Xin Zhao, Lihao Wu, Qinghua Zhang. (2013) In situ growth of ordered polyaniline nanowires on surfactant stabilized exfoliated graphene as high-performance supercapacitor electrodes. Synth. Met. 185-186:89-95.

[26]. Muhammad Faisal and Syed Khasim. (2013) Electrical conductivity, dielectric behavior and EMI shielding effectiveness of polyaniline-yttrium oxide composites. Bull. Korean Chem. Soc. 34:99-106.

[27]. Jiahua Zhu, Suying Wei, Lei Zhang, Yuanbing Mao, JongeunRyu, Amar B. Karki, David P. Younge, Zhanhu Guo. (2011) Polyaniline-tungsten oxide metacomposites with tunable electronic properties. J. Mater. Chem. 21:342-348.

[28]. Y.T. Ravikiran, M.T. Lagare, M. Sairam, N.N. Mallikarjuna, B. Sreedhar, S. Manohar, A.G. MacDiarmid, T.M. Aminabhavi. (2006) Synthesis, characterization and low frequency AC conduction of polyaniline/niobium pentoxide composites. Synth. Met. 156:1139-1147.

[29]. Javed Alam Khan, MohdQasim, Braj Raj Singh, Sneha Singh, MohdShoeb, Wasi Khan, Dibakar Das, Alim H. Naqvi. (2013) Synthesis and characterization of structural, optical, thermal and dielectric properties of polyaniline/$CoFe_2O_4$ nanocomposites with special reference to photocatalytic activity. Spectr. Acta Part A: Mol. and Bio. Spectr. 109:313-321.